Elucidating the Nanoscale Structure of Dinosaur Bone

E. M. Boatman,[1] * R. Gronsky,[1] M. B. Goodwin,[2] and R. O. Ritchie[1]
[1]Department of Materials Science and Engineering, University of California, Berkeley, CA 94720
[2]Museum of Paleontology, University of California, Berkeley, CA 94720
*elizabeth_boatman@berkeley.edu

Introduction

Bone is an important material in many scientific disciplines because of its unique structure-property relationships, which are intrinsically dependent on its nanoscale components, bioapatite and collagen. As a living tissue, bone has evolved over hundreds of millions of years, and most vertebrates are now extinct. However, the vast majority of the relevant literature has engaged only modern bone tissues, neglecting the deep time perspective. Why?

In exceptional circumstances, we recover the bones of extinct animals as fossils, which have suffered chemical, biological, and physical changes known as diagenetic alteration. Such changes often include permineralization or the enrichment/depletion of particular elements [1]. Even though fossilization is increasingly recognized as preservational and not necessarily destructive, with evidence of preserved proteins in dinosaur specimens lending support to this changing perspective [2][3], nonetheless the changes introduced by fossilization ultimately preclude our ability to test the mechanical properties of ancient bones directly.

Instead, there exists the potential to back-infer the mechanical behavior of ancient bone tissues based on the direct mechanical testing of modern structural analogs. We believe that many fields of scientific inquiry, from evolutionary biology to medicine to materials engineering, would significantly benefit from such paleontological advances.

For example, various investigators have explored the mechanical performance of dinosaur skulls during head butting [4] and biting [5] behaviors using a combination of computed tomography and computer-based modeling approaches. Many higher-order features of bone structure (for example, tissue type and remodeling rates) have been extensively demonstrated in both modern and fossil bone tissues, used to develop models of ontogenetic growth [6], or used to understand better the biomineralization of tissues, such as tendon [7]. Additionally, because the features of bone reflect the physiology of the respective organism, thoughtful inspection of the tissues of ancient organisms may further elucidate the origin of homeothermy, the gigantic growth of megafauna, and the origin of flight in birds. Materials biomimicry studies of other biomineralized tissues of interest already have incorporated a deep time aspect (for example, antler [8] and fish scale [9]).

To a degree, progress in this area remains hindered by our limited ability to identify the original structures in fossil bone or other biomineralized tissues at all relevant length scales. Further, the nanoscale structure of bone remains relatively underexplored in the overall literature on bone, detracting from our ability to explore fully the questions under investigation in the variety of examples given above. Ultimately, the nanoscale structure of bone is the foundational basis for all higher-order structures of bone tissue. In the presumed absence of collagen, as a result of diagenesis, investigations of the structure of ancient bone tissues must rely exclusively on the preservation of bioapatite. Hence, the goal of this investigation is to measure the relevant nanoscale parameters, including bone mineral phase, size, morphology, and relative spatial orientation (that is, the microfibrillar dimensions).

Materials and Methods

A set of four fossil specimens (see Table 1) was identified for analysis, with three modern analogs, in accordance with the extant phylogenetic bracketing (EPB) technique [10], which presents a framework for inferring the identities of soft tissues typically lost during fossilization. The protocol is based on the thorough observation of tissues in modern, closely related groups, which are used to establish a phylogenetic bracket by selecting a direct evolutionary descendent (that is, Palaeognathae: ostrich and *Rhea*) and an evolutionary outgroup (that is, Crocodilia: *Caiman*).

Transverse polished specimens were analyzed with electron microprobe (Cameca SX-100) wavelength-dispersive spectrometry (WDS), quantified for typical bioapatite elements and elements commonly known to enrich ancient bones. Locations of analysis were identified in regions of comparative isolation, midway between osteons (blood vessel channels). X-ray diffraction (XRD, Rigaku MiniFlex II at 30 kV and 15 mA) also was performed to identify the mineral phase(s) present.

Increased porosity and loss of collagen occur in bone as a result of fossilization, acting as perforation and potentially yielding microfibrillar structures via mechanically destructive preparation. Hence, fossil specimen fragments were pulverized in 95% ethanol and dispersed on ultrathin carbon on holey carbon Cu grids. The dispersed fragments were imaged by transmission electron microscopy (TEM, JEOL 2011) at 200 keV.

Table 1: The identities and ages of the specimens used in this study, provided by the UC Museum of Paleontology.

Age	Identity	Element	Specimen No.
modern	ostrich	femur	125001
modern	*Rhea*	femur	129668
modern	*Caiman*	femur	63533
Eocene	*Pristichampsus*	femur	170767
Late Cretaceous	hadrosaur	radius	175247
Late Cretaceous	hadrosaur	femur	169073
Late Cretaceous	*Tyrannosaurus*	femur	136517

The SPI Supplies Family of Instruments

Excellence in sample preparation
just a click away... 2spi.com

Your results will never be better than your sample preparation. See how SPI Supplies can help you deliver the highest quality results for all your SEM/EDS, TEM and FESEM applications.

1. **Osmium Plasma Coaters** for FESEM Applications
2. **SPI-MODULE™** Sputter/Carbon Coater Module
3. **Gentle Mill™** Ion Milling System
4. **Plasma Prep™ III** Solid State Plasma Cleaner for cleaning TEM holders
5. **Plasma Prep™ X** Parallel Plate Plasma Etcher
6. **Plasma Prep™ III** Plasma Etcher with **PPIII Process Controller**
7. **Vacu Prep™ II** Turbo Pump Evaporation System
8. **SPI-DRY™** Critical Point Dryer
9. **Precision Spin Coater** Spin coater

SPI SUPPLIES®

SPI Supplies Division of **STRUCTURE PROBE, Inc.**

P.O. Box 656 • West Chester, PA 19381-0656 USA
Phone: 1-610-436-5400 • 1-800-2424-SPI (USA and Canada) • Fax: 1-610-436-5755 • 2spi.com • E-mail: sales@2spi.com

Small-angle X-ray scattering (SAXS) was used to identify two key aspects of the bone microfibril. The D-spacing of type I collagen arises from a characteristic stacking pattern of collagen molecules, yielding a repeat spacing of 67 nm that is conserved throughout the vertebrates; this molecular arrangement, and associated protein cross-links, is critical for both the strength and compliance of vertebrate structural tissues. SAXS is frequently used to investigate changes in the D-spacing of modern tissues following mechanical manipulation [11]. Further, close-packed bundling within the microfibril and its width can be identified using SAXS [12]. Accordingly, thin sections of the specimens were analyzed in a transmission arrangement using a Bruker AXS NANOSTAR at 40 kV and 35 mA.

Results and Discussion

In all cases, XRD analysis yields patterns consistent with apatite. Data from *Tyrannosaurus* (Figure 1) are shown as an example, including both a bulk specimen profile exhibiting a high degree of preferred orientation and powdered *Tyrannosaurus* bone, in which the diffraction peaks are more pronounced and easier to index. The poor structure of the peaks is attributed to the extensive nanocrystallinity within the specimen (see TEM results, below) and the inherently impure nature of bioapatite.

Certain elements readily substitute in exposed bioapatite over time. Fluorine enrichment to 1.9–3.8 at.%, which is a common occurrence in fossil bone [13], was found throughout the fossil specimens, as indicated by the WDS results (Figure 2 inset (b)). The apatite class of minerals includes a set of stoichiometric variants, of which hydroxyapatite ($Ca_{10}(PO_4)_6(OH)_2$) and fluorapatite ($Ca_{10}(PO_4)_6F_2$) are end-members, with a complete solid solution existing between them. Fluorine readily displaces hydroxide groups within the apatite lattice; hence, in the medical context, this phenomenon is referred to as the bone-seeking behavior of fluoride ions. However, because the lattice parameters of these two minerals are nearly identical, fluoride substitutions alone impart minimal lattice strain (no structural changes) in fossil bioapatite; they merely serve as an indicator of chemical diagenetic alteration.

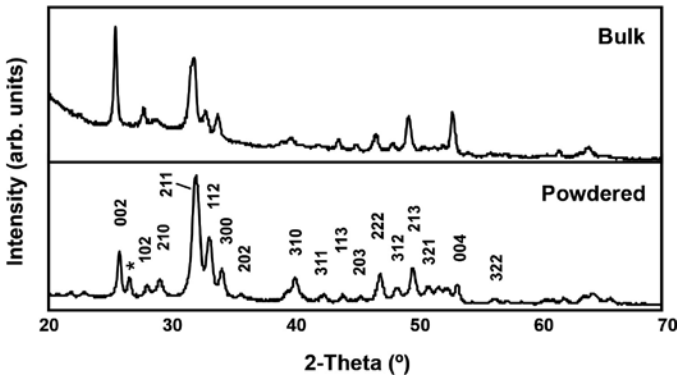

Figure 1: Example XRD patterns of bulk and powdered *Tyrannosaurus* bone. The presence of additional, more defined peaks in the powdered pattern indicates that the bulk bone specimen contains a high degree of preferred orientation. There is one spurious peak present at approximately 26° (*); otherwise, the pattern reproduces that of modern bioapatite. The general poor quality of the diffraction peaks is the result of nanocrystallinity (see TEM images in Figure 4) and the impure nature of the bioapatite structure (see WDS results in Figure 2).

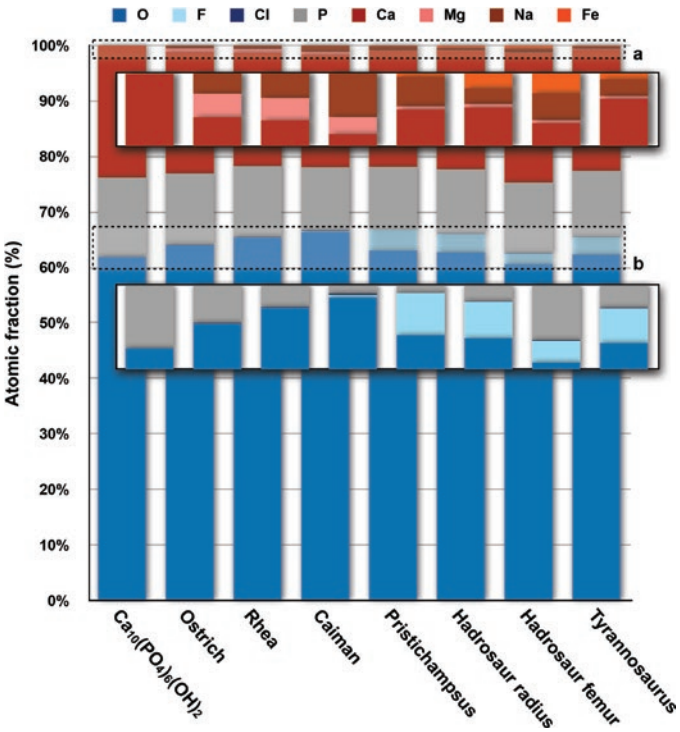

Figure 2: A summary of the modern and fossil bone compositions following WDS analysis. Modern bioapatite (ostrich, *Rhea*, *Caiman*) is impure $Ca_{10}(PO_4)_6(OH)_2$ and commonly contains minor enrichment in F, Na, and Mg. Fluorine enrichment to 1.9–3.8 at.% was found throughout the fossil specimens. Fossil bone enrichment in Fe and loss of Mg also can be observed. The values are reported as atomic fractions of 100%.

Other significant compositional changes in these specimens include enrichment in Fe and loss of Mg (Figure 2 inset (a)). In particular, Fe is often incorporated into fossil bone in the form of oxides/sulfides, as highlighted in recent studies on the possible role of Fe in fossil soft tissue preservation [14]. Partial cation exchange may occur in bioapatite exposed to ground waters over time; however, the changes observed here may suggest a balancing effect and are minimal.

Whether bioapatite is preserved in fossil specimens in any meaningful form, and consequently the nanoscale structure, remains a point of contention in the paleontological literature. Our combined XRD and electron microprobe WDS results indicate that bioapatite is preserved in these specimens, albeit in a chemically altered form that is readily identifiable. However, additional techniques, such as TEM imaging, are critical for complete characterization, because the morphology and arrangement of bioapatite in compact bone are key parameters in studies of modern bone.

TEM analysis was performed to assess directly the state of preservation of nanoplates and microfibrillar structures in the fossil specimens. Bright-field inspection highlights the extensive presence of nanocrystalline forms (Figure 3), as documented for other fossil bones [15], further supporting our interpretation of the XRD results presented above. Biological apatite is uniquely identified as plate-shaped nanocrystallites, which are critical for bone strength; in contrast, geological apatite tends to form comparatively large hexagonal prisms. Beyond the extensive presence of nanoplates, SAED investigation of fossil

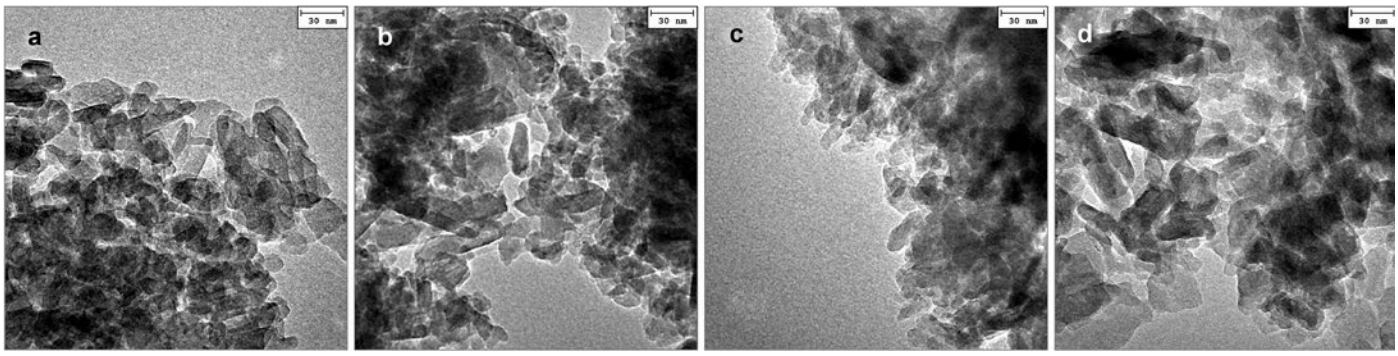

Figure 3: All fossil specimens exhibit extensive nanocrystallinity in TEM bright-field images (collected at 5,000×): (a) *Pristichampsus*, (b) hadrosaur radius, (c) hadrosaur femur, and (d) *Tyrannosaurus*.

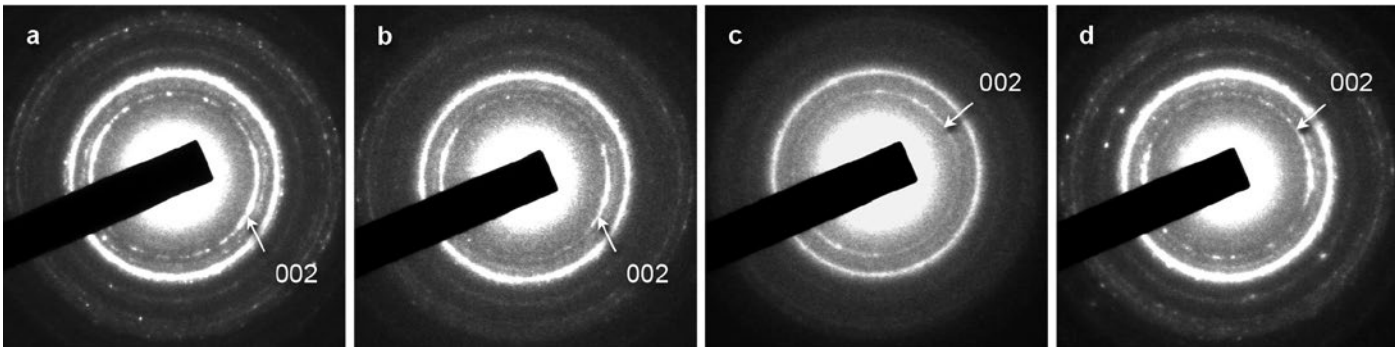

Figure 4: Fragments of fossil bone tissue were investigated by SAED, and representative diffraction patterns are presented for (a) *Pristichampsus*, (b) hadrosaur radius, (c) hadrosaur femur, and (d) *Tyrannosaurus*. All recorded diffraction patterns are consistent with bioapatite, based on indexing of the partial rings (hydroxyapatite 002, white arrows), which indicate a high degree of preferred orientation.

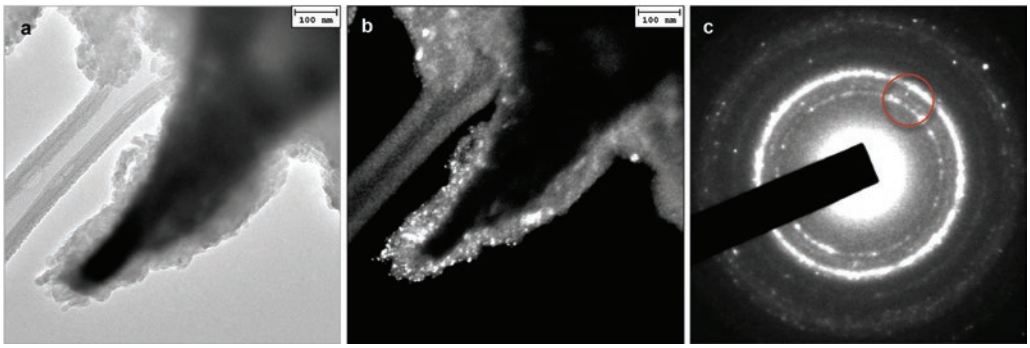

Figure 5: (a) A tubular projection from a *Pristichampsus* fragment, interpreted as a microfibrillar section. (b) A dark-field image generated from (c) the corresponding diffraction pattern (red circle indicates the location and size of the displaced objective aperture). Nanocrystallinity is apparent in the dark-field image.

bone fragments reveals a high degree of preferred orientation (Figures 4(a)–(d)), consistent with patterns obtained from modern mineralized tissues and individual fibrils [16].

Pulverized/dispersed fossil bone samples frequently yield protruding fragments or tubular sections (for example, Figure 5(a)), interpreted as portions of microfibrils. The presence of nanocrystalline forms is identifiable using dark-field techniques (Figure 5(b)), with the corresponding diffraction pattern given in Figure 5(c). In this work, dark-field techniques confirm the thickness of the fossil nanoplates to be 2–4 nm; modern bioapatite nanoplates are routinely identified in this same thickness range [17]. In sum, these TEM results not only reinforce our understanding that the fossil bioapatite in these specimens is *minimally altered,* but they also demonstrate the high degree of localized, preferred orientation in the compact bone tissues of these extinct species, reinforcing our understanding that collagen/bioapatite orientation has evolved as a key aspect of performance in load-bearing bone.

Our interpretation of the TEM results is further supported by SAXS analysis. The whole patterns (Figure 6) for the three modern bones and for the fossil *Tyrannosaurus* and hadrosaur radius specimens exhibit distinctly elliptical shapes, consistent with a high degree of preferred orientation; additionally, a partial 002 ring is apparent in the hadrosaur radius sample, indicating nanoscale structural preservation over a relatively large area (the beam is micrometer-size). For several of the fossil bone tissues, SAXS line profile analysis (Figure 7) yields small peaks at approximately 39 nm (inset (b1)), representing dense stacks of nanoplates, and at 23 nm (inset (b2)), which is the region of collagen overlap in modern bones but is a porous cavity in fossils. These values sum to nearly 67 nm, while the accepted values of these features are 40 nm and 27 nm, respectively, in modern bone tissue.

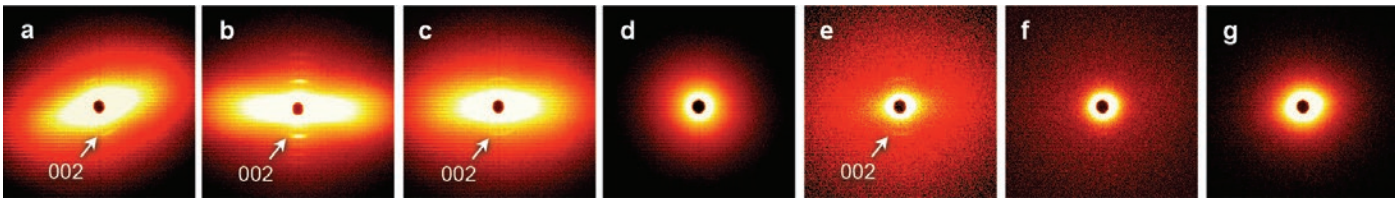

Figure 6: SAXS whole patterns for modern and fossil bone specimens. Elliptical shapes, visible for modern bones in addition to hadrosaur radius and *Tyrannosaurus*, are consistent with a high degree of preferred orientation. Partial *c*-axis 002 rings (white arrows) are readily visible for modern bones and hadrosaur radius. (a) Ostrich, (b) *Rhea*, (c) *Caiman*, (d) *Pristichampsus*, (e) hadrosaur radius, (f) hadrosaur femur, and (g) *Tyrannosaurus*.

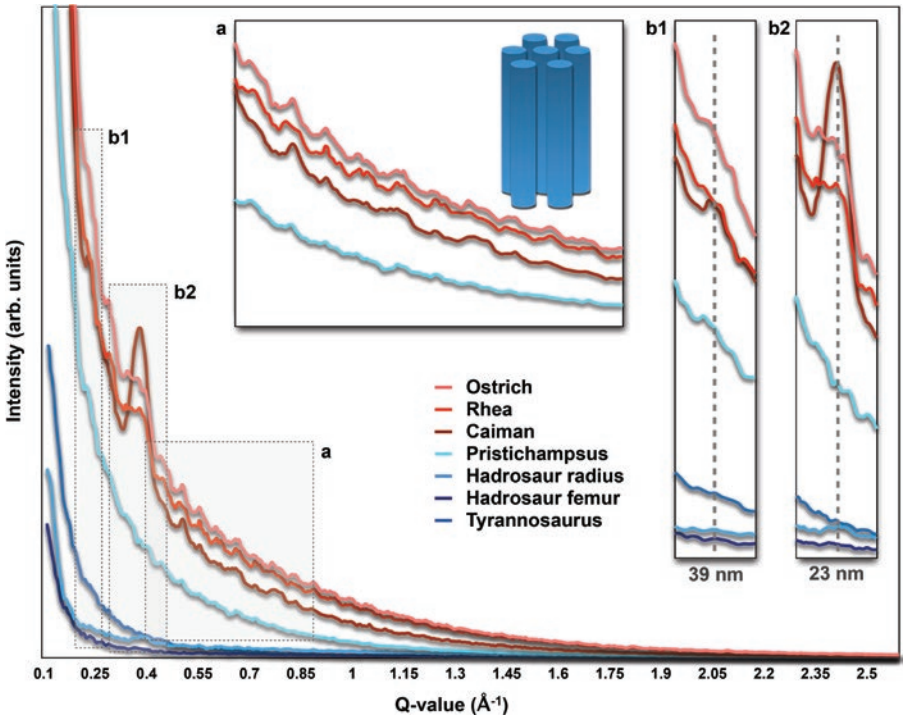

Figure 7: SAXS line profiles (partial integration of whole pattern pie wedges from −5–25°) plotted against Q-value ($Å^{-1}$). Computer simulation of the microfibrillar structure was performed in [12], indicating that close-packed bundling (array of blue "microfibrils" in inset (a)) yields an overlying oscillatory pattern, which may be visible in the enlarged profile sections detailed in inset (a). Small peaks centered at 0.016003 $Å^{-1}$ = 39 nm (inset (b1)) and 0.027027 $Å^{-1}$ = 23 nm (inset (b2)) approximately represent the gap (40 nm, in which dense stacks of nanoplates tend to form) and overlap (27 nm, a void space in these fossil tissues, following collagen loss) regions in the type I collagen structure.

The overlying oscillatory pattern evident in one SAXS fossil line profile and all three modern bones provides additional information (Figure 7 inset (a)). This oscillation is produced by the close-packing of microfibrils within the fibrillar structure [12]. Its presence indicates that this fossil bioapatite retains the bundling character of the original microfibrillar structure over a significant distance. Careful measurement of the peak-to-peak distance yields an average microfibril width of 147.3 nm for the *Pristichampsus* specimen.

Conclusions

In this study, microscopy and microanalysis techniques, including analyses with both electron and X-ray beams, were applied to modern and fossil compact bone tissues to demonstrate the feasibility of applying modern bone characterization techniques to fossil/dinosaur tissues, while specifically investigating preserved nanoscale structure. It was found that, despite chemical alteration (for example, enrichment in F and Fe, loss of Mg), the bioapatite mineral phase is retained with minimal changes in plate-like, nano-crystalline morphologies. These results suggest that neither significant coarsening nor dissolution/reprecipitation have occurred as a result of diagenesis. TEM observations and SAXS analyses further support the identification of microfibrillar structures, including the extraction of a microfibrillar width from one fossil specimen.

These combined data represent some of the first measurements of nanoscale structure in fossil dinosaur bone, contributing to our understanding of bone from the deep time perspective and reinforcing the perspective that fossilization is a preservational process. Beyond these specimens, the vertebrate fossil record represents a vast repository of novel tissues, structural adaptations, and evolution. Our ability to analyze these ancient bone tissues at the nanoscale has the potential to enhance significantly the research objectives of evolutionary biologists, paleontologists, the medical disciplines, and materials engineers.

Acknowledgments

We are thankful for the resources and capabilities supplied by the UC Davis Electron Microprobe Laboratory and the research group of Prof. Paul Alivisatos at UC Berkeley, who provided access to SAXS instrumentation. We also acknowledge the funding received from the Jurassic Foundation and UC Berkeley.

References

[1] MB Goodwin, PG Grant, G Bench, and PA Holroyd, *Palaeogeogr Palaeocl* 253 (2007) 458–76.

[2] MH Schweitzer, W Zheng, CL Organ, R Avci, Z Suo, LM Freimark, VS Lebleu, MB Duncan, MG Vander Heiden, JM Neveu, WS Lane, JS Cottrell, JR Horner, LC Cantley, R Kalluri, and JM Asara, *Science* 324 (2009) 626–31.

[3] RA Wogelius, PL Manning, HE Barden, NP Edwards, SM Webb, WI Sellers, KG Taylor, PL Larson, P Dodson, H You, L Da-qing, and U Bergmann, *Science* 333 (2011) 1622–26.

[4] E Snell and A Cox, *Palaeontol Electronica* 11(1) (2008) 3A.

[5] EJ Rayfield, *Proc R Soc Lond B* 271 (2004) 1451–59.
[6] PM Sander, *Palaeobiology* 26(3) (2000) 466–88.
[7] JS Adams and CL Organ, *J Vertebr Paleontol* 25(3) (2005) 614–22.
[8] RM Kulin, P-Y Chen, F Jiang, J McKittrick, and KS Vecchio, *JOM* 62(1) (2010) 41–46.
[9] J Song, C Ortiz, and MC Boyce, *J Mech Behav Biomed* 4 (2011) 699–712.
[10] LM Witmer, *Functional Morphology of Vertebrate Paleontology*, ed. Jeff Thomason, Cambridge University Press, New York, 1995.
[11] HS Gupta, J Seto, W Wagermaier, P Zaslansky, P Boesecke, and P Fratzl, *PNAS* 103(47) (2006) 17741–46.
[12] H Suhonen, M Fernández, R Serimaa, and P Suortti, *Phys Med Biol* 50(22) (2005) 5401–16.
[13] J Elorza, H Astibia, X Murelaga, and X Pereda-Suberbiola, *Cretaceous Research* 20 (1999) 169–87.
[14] MH Schweitzer, Z Suo, R Avci, JM Asara, MA Allen, FT Arce, and JR Horner, *Science* 316 (2007) 277–80.
[15] M Dumont, A Kostka, PM Sander, A Borbely, and A Kaysser-Pyzalla, *Palaeogeogr Palaeocl* 310(1–2) (2011) 108–16.
[16] W Traub, T Arad, and S Weiner, *Proc Natl Acad Sci USA* 86 (1989) 9822–26.
[17] S Weiner and W Traub, *The FASEB Journal* 6(3) (1992) 879–85.

MT